

Spontaneous Ignition Behavior of *n*-Decane Fuel Droplet Array near Ignition Limit

Masanori SAITO¹, Yurie OHNO¹, Hiroataka KATO¹, Yusuke SUGANUMA²,
Masato MIKAMI³, Masao KIKUCHI⁴, Yuko INATOMI⁵, Takehiko ISHIKAWA⁵,
Osamu MORIUE⁶, Hiroshi NOMURA² and Mitsuaki TANABE¹

Abstract

A microgravity experiment utilizing sounding rocket is going to be held in 2021 to clarify cool flame occurrence from *n*-decane droplet array near spontaneous ignition limit. As a preliminary study for the experiment, the 2D numerical simulation is carried out. The almost identical numerical geometry to the actual furnace for the rocket experiment is used to predict the cool flame occurrence in the rocket experiment. The interference of the droplets is validated by calculation with different inter-droplet distance. The employed fuel is *n*-decane of 1.0 mm in diameter. The initial temperature and pressure are 550 K and 1 atm respectively. The results shows that the cool flame occurs from the outside of the fuel droplet array. A fuel concentration at inter-droplet is higher than the outer side, whereas the temperature at inter-droplet is lower than the outer side. It is thought that the lower temperature yields increase in the spontaneous ignition delay time surpassing the shorten effect of the ignition delay time due to higher fuel concentration.

Keyword(s): Cool flame, Droplet array, Spontaneous ignition, Sounding rocket.

Received 21 December 2018, Accepted 1 April 2019, Published 30 April 2019

1. Introduction

Spray combustion is utilized to many kind of internal combustion engines such as a Diesel engine and a rocket engine. Fuel is combusted subsequent to the process of atomization, vaporization and spontaneous ignition. To clarify these physical and chemical process is important to predict the flame position in a combustion chamber, ignition timing, soot formation etc.

Diesel engine, for instance, utilizes PCI combustion to reduce both NO_x and soot emission¹). On the other hand, it is difficult to control the ignition timing because the ignition timing is not injection timing but is late for the injection due to necessity of evaporation time to make homogenized mixture.

In the case of the combustion oscillation in a rocket combustor, it onsets when the heat release fluctuation couples pressure fluctuation. Because the heat release timing is controlled by the ignition timing, spontaneous ignition is the key phenomenon to control the combustion oscillation.

In the case of hydrocarbon fuel, the occurrence of a cool flame has been observed before appearance of luminance flame²). The induction time to the appearance of luminance flame called second induction time has temperature dependency. Since the temperature increases as a result of cool flame, the second induction time is affected by the induction time to the appearance

of the cool flame called first induction time. Therefore, the prediction of the cool flame generation is very important to predict the combustion process of the hydrocarbon fuel and huge number of the ignition experiment have been carried out for the modeling of the spray combustion. The simplest model of the spray combustion is the single droplet combustion. Furthermore, the microgravity experiment is usually conducted to simplify the model because the natural convection which changes the ignition characteristics³) can be negligible and the ignition phenomena of the single droplet can be assumed to be spherical symmetry. To be able to consider the spherical symmetry provides an advantage on the lower calculation cost. Moreover, the large droplet usually utilizes to observation of the spontaneous ignition behavior, whereas the ignition characteristic of the large droplet is strongly affected by the natural convection. Therefore, the microgravity environment is usually used to verify the spontaneous ignition characteristics.

To make a microgravity environment, a drop tower is widely used. Kumagai et al. carried out the world first experiment of suspended single droplet combustion by using drop tower⁴). The multiple droplets exist in an actual combustor and hence the interference of droplets is need to be considered. Moriue et al.⁵) conducted the microgravity experiment for *n*-decane droplet pair ignition by using drop tower. They found that the cool flame

1 College of Science and Technology, Nihon University, 7-24-1 Narashinodai, Funabashi, Chiba 274-8501, Japan.

2 College of Industrial Technology, Nihon University, 1-2-1 Izumi-cyo, Narashino, Chiba 275-8575, Japan.

3 Graduate School of Science and Technology for Innovation, Yamaguchi University, 2-16-1 Tokiwadai, Ube, Yamaguchi 755-8611, Japan.

4 Japan Aerospace Exploration Agency, 2-1-1 Sengen, Tsukuba, Ibaraki 305-8505, Japan.

5 Japan Aerospace Exploration Agency, 3-1-1 Yoshinodai, Chuo-ku, Sagamihara, Kanagawa 252-5210, Japan School of Physical and Sciences, SOKENDAI (The Graduate University for Advanced Studies), 3-1-1 Yoshinodai, Chuo-ku, Kanagawa, Sagamihara, 252-5210, Japan.

6 Faculty of Engineering, Kyushu University, 744 Motoooka, Nishi-ku, Fukuoka 819-0395, Japan.

(E-mail: saito@aero.cst.nihon-u.ac.jp)

ignition delay and cool flame temperature increase with decrease in inter-droplet distance. Eigenbrod et al. conducted formaldehyde LIF diagnostics in microgravity environment using drop tower Bremen⁶). They found that the ignition delay time of the droplet pair strongly depends on the droplets distance.

On the other hand, the duration of the drop tower is not long enough to get the ignition behavior near the ignition limit due to longer induction time and it have not been clarified yet. The data near the ignition limit is very important not only because the data is lacking but also because it is able to validate the influence of the species transport due to longer ignition delay time. Therefore, a rocket experiment is necessary to obtain the ignition limit characteristics. As a micro-gravity experiment utilizing a rocket or space environment which can realize the longer microgravity time than the conventional drop tower, "PHOENIX-I" mission by TEXUS46 was launched in 2009. This mission aimed to clarify the partially pre-vaporization of fuel droplet array⁷). Mikami et al investigated the flame spread after ignition of the droplets arranged in 2D lattice randomly at "KIBO" of the ISS module⁸⁻¹⁰). Farouk et al. also utilizes the ISS to observe the cool flame of isolated *n*-heptane^{11, 12}). They found the transition to a cool flame from the hot flame.

To clarify the cool flame occurrence near ignition limit of the fuel droplet, "PHOENIX-II" project¹³) is in progress as international collaboration project between Japan and Germany. In the experiment, sounding rocket which can produce the microgravity environment for about 6 minutes will be utilized to clarify the effect of inter-droplet interference for the cool flame generation near ignition limit. For the preliminary study, the numerical calculation of the *n*-decane droplet ignition is carried out to obtain the ignition delay time of the droplets existing the inter-droplet interference.

2. Microgravity Experiment by TEXUS Rocket

2.1 Experimental Systems of Droplet Array Combustion Unit (DCU)

The draft layout of the droplet array combustion unit (DCU) of an experimental module for the rocket experiment is shown in Fig. 1. To carry out the ignition limit experiment as close as possible, two different temperature conditions near ignition limit of 570 ± 2.5 K and 590 ± 2.5 K are chosen as the ambient temperature. The DCU has two furnaces ($119 \text{ mm} \times 57 \text{ mm} \times 42 \text{ mm}$ in inner dimension) with optical access windows and the experiment can be carried out with different ambient temperature simultaneously within the limited flight duration. The employed fuel is *n*-decane droplet of 1.0 ± 0.05 mm in diameter. An intensified high-speed camera (HICAM 500, Lambert Instruments BV) will be used to catch the weak HCHO chemiluminescent whose wave length of 392.4 nm from cool flame.

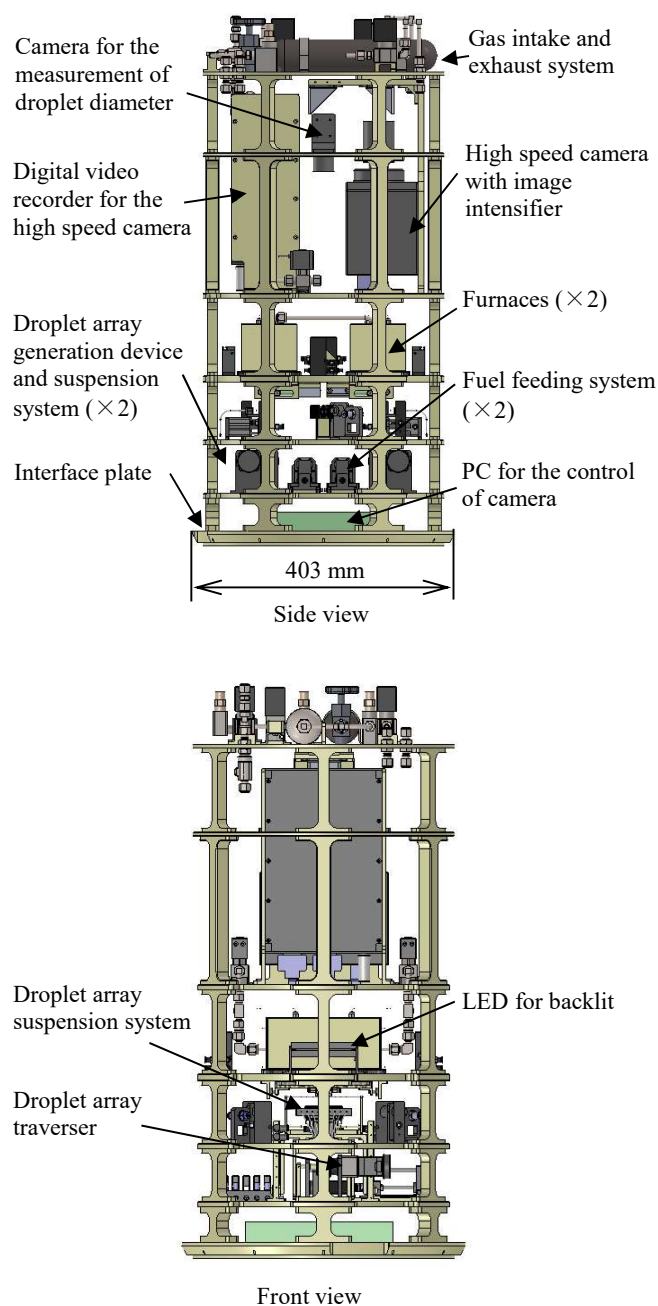


Fig. 1 Draft layout of the droplet array combustion unit (DCU).

Figure 2 shows the developed droplet array suspension system. The fiber structure originates from Nomura's work¹⁴). Two SiC fibers of 14 μm in diameter are arched and crossed. The droplet can be suspended at an intersection of each fibers. The suspension system can suspend droplets up to 9 with inter-droplet distance of 8 mm. By suspending of droplet at the top of the droplet suspension system, the influence of the flow induced by the surrounding structure during insert to furnace can be minimize. The suspender can be elevated by droplet array traverser from the inlet of the furnace to the experimental position within 0.1 s which is short enough to neglect the reaction during insert.

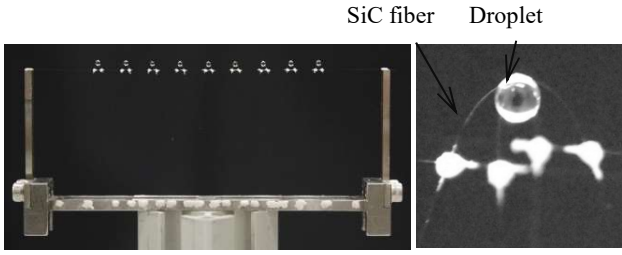


Fig. 2 Suspended *n*-decane droplet array (left) and the magnified view of a suspended fuel droplet (right).

3. Numerical Modeling of Droplets Ignition for the Flight Experiment

3.1. Numerical Conditions

Droplet pair and droplet array ignitions are modeled and predicted by 2D CFD for the preparation of the flight experiment. Two dimensional axisymmetric unsteady calculation is carried out. A reduced *n*-decane reaction model including 77 species and 287 reactions developed by Qiu *et al.*¹⁵⁾ is employed for the reaction model. The ambient gas is still air. To emphasize the effect of the transport of the intermediate species on the ignition process, the initial temperature of the air is set to 550 K which is the longer ignition delay time condition than the actual experiment temperature of 570 K and 590 K. The ambient pressure is set to 1 atm. A numerical domain is shown in **Fig. 3**.

The size of the numerical domain is set to 28 mm × 57.5 mm. A bottom boundary is axisymmetric boundary and a left boundary is symmetric boundary. Top and right walls of the numerical domain is set to 550 K of isothermal wall. Droplet surfaces are fixed boundary of mass flow inlet whose radius is 0.5 mm corresponding to the initial droplet diameter $d_0 = 1.0$ mm and liquid state is not considered to simplify the calculation. The inter-droplet distance D was changed from 8 mm to ∞ mm (single droplet). In the case of the droplet array, the numerical domain with 8 mm inter-droplet distance is shown in **Fig. 3**. The inter-droplet distance of 8 mm and 16 mm are analyzed. **Figure 4** shows the simple vaporization model. The mass flow rate of the *n*-decane is determined in accordance with the simple model of the time variation of the fuel droplet diameter d and surface temperature which is calculated by the vaporization rate of 0.1 mm²/s referred from the past work¹⁶⁾. The mass flow rate is calculated by the following formula.

$$\dot{m} = \frac{\pi \rho K}{4} \sqrt{-Kt + d_0^2} \quad (1)$$

Where K is the vaporization rate and ρ is density of *n*-decane ($=7.3 \times 10^{-7}$ kg/mm³). The calculation time step is 1.0×10^{-3} s. To obtain a reference data without species diffusion, 0D reaction calculation is also carried out with the same reaction model to the 2D calculation.

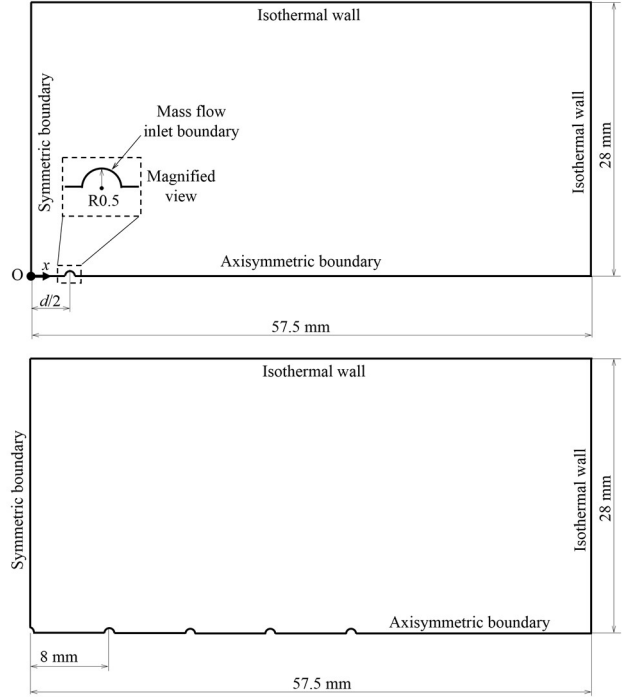


Fig. 3 Numerical domain (upper figure: droplet pair, lower figure: droplet array).

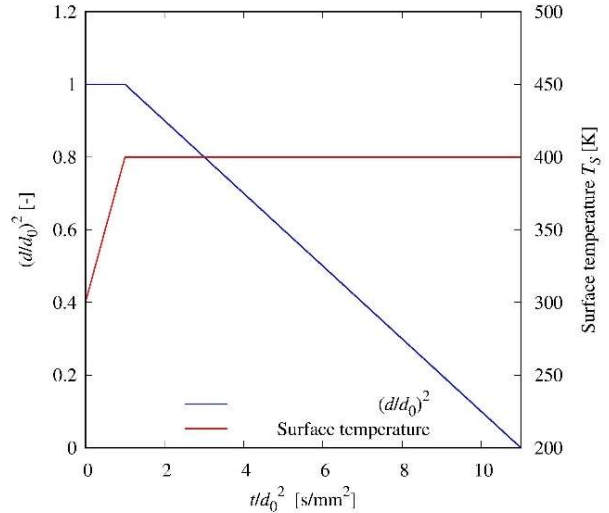


Fig. 4 Time history of the *n*-decane droplet diameter and temperature for numerical simulation.

3.2 Ignition Delay Evaluation

Figure 5 shows a temperature time history. The temperature is the maximum temperature in the calculation domain. Time zero corresponds with the start of a calculation. After some induction time, the temperature rises as a result of a cool flame generation. Ignition delay time τ_i is defined as the period from a calculation start time to the time when dT/dt takes maximum.

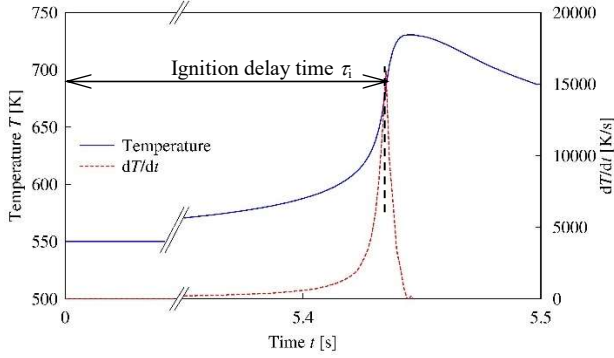


Fig. 5 Typical temperature and temperature rise rate history of *n*-decane droplet ignition.

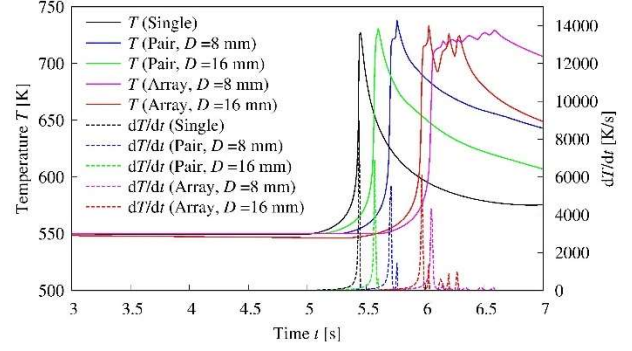


Fig. 7 Relationship between temperature history and inter-droplet distance.

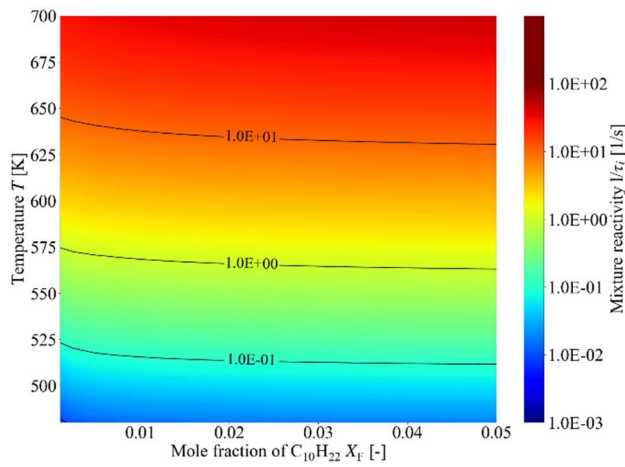


Fig. 6 Dependence of ambient temperature and fuel mole fraction on reactivity of mixture.

4. Results and Discussion

4.1 Mixture Reactivity

The ignition delay time of the cool flame depends on the ambient temperature and fuel concentration. A reciprocal of the ignition delay represents reaction rate, i. e. mixture reactivity. The high reactive mixture gives the short ignition delay time, and vice versa. To identify the ignition point of the cool flame, the mixture reactivity shown in **Fig. 6** is calculated by the 0D reaction calculation. The 0D calculation does not consider diffusion of each species and heat, the result is used for the comparison with the 2D calculation as the reference data. The contour of the graph shows the mixture reactivity represented by $1/\tau_i$. The mixture reactivity for the occurrence of the cool flame becomes high with increase in ambient temperature and $C_{10}H_{22}$ mole fraction X_F . Besides, the influence of the mole fraction on the mixture reactivity is small compared with the influence of the ambient temperature.

The ignition delay time of the single droplet, droplet pair whose inter-droplet distance is changed, and droplet array were

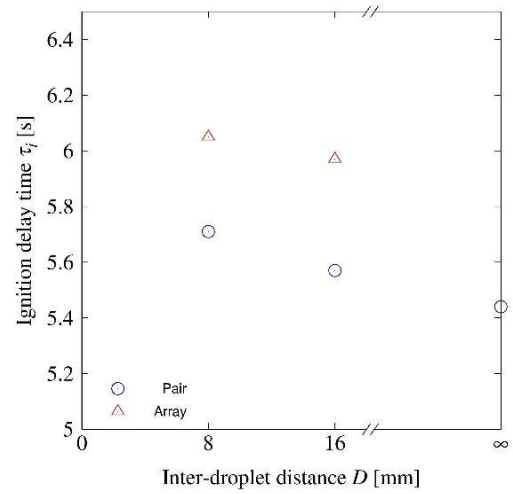


Fig. 8 Relationship between ignition delay time and inter-droplet distance.

calculated by CFD. **Figure 7** shows the time history of temperature and temperature rise rate. In the case of the single droplet, the graph shows the single spike due to the single heat release. The temperature rise rate of droplet pair in 8 mm inter-droplet distance shows the bimodal spike. In the case of the droplet array with $D = 16$ mm, the triple peak is found because the 5 droplets ignite sequentially. On the other hand, the flat temperature history is found in droplet array of $D = 8$ mm due to close inter-droplet distance and heat release occurs within the heat dissipation. From these results, we define the time before ignition τ_{90} as 90 % time of the ignition delay time because no temperature rising is found.

Figure 8 shows the ignition delay time with different inter-droplet distances.

The distance of infinity corresponds with the ignition delay time of a single droplet. The ignition delay time of 6.05 s in 8 mm inter-droplet distance of droplet array condition is the longest in the other conditions. The ignition delay time becomes short with increase in the inter-droplet distance. In the case of the droplet

pair, the ignition delay time of 5.71 s in 8 mm inter-droplet distance is longer than that of 16 mm. The ignition delay time decreases with increase in the inter-droplet distance as well as droplet array condition. This tendency corresponds with the past work^{5,6}). The ignition delay time of the single droplet is 5.44 s which is the shortest ignition delay time in the all conditions.

4.2 Ignition Point and Distribution of Intermediate Species

Figure 9 shows the temperature distribution along axisymmetric boundary of the single droplet condition. The coordination zero corresponds with the symmetric boundary. At τ_{90} , the lower temperature than the ambient temperature is found due to the low temperature fuel in the vicinity of the droplet surface. As increase in the distance from the droplet surface, temperature increases gradually. At ignition delay time of 5.44 s, temperature starts to rise at $x = 5$ mm. The maximum temperature of 724 K is taken at $x = 3.5$ mm which is 3.0 mm apart from the droplet surface at $t = 5.45$ s. After temperature rising, the maximum temperature point moves inward.

Figure 10 shows the time series of the mole fraction of $C_{10}H_{22}$ along axisymmetric boundary. The fuel mole fraction starts to decrease before ignition delay time. At ignition delay time, significant consumption of fuel was found around $x = 3$ to 4 mm where temperature rises. Comparing $t = 5.44$ s and $t = 5.45$ s just after ignition delay time, it is found that the fuel is consumed toward droplet.

From the result of **Fig. 9** and **10**, it is found that the temperature rising starts around the position of $X_F = 0.0065$ of fuel leaner side at τ_{90} . The temperature at τ_{90} corresponding with $X_F = 0.0065$ position is approximate 540 K. With decrease in distance from

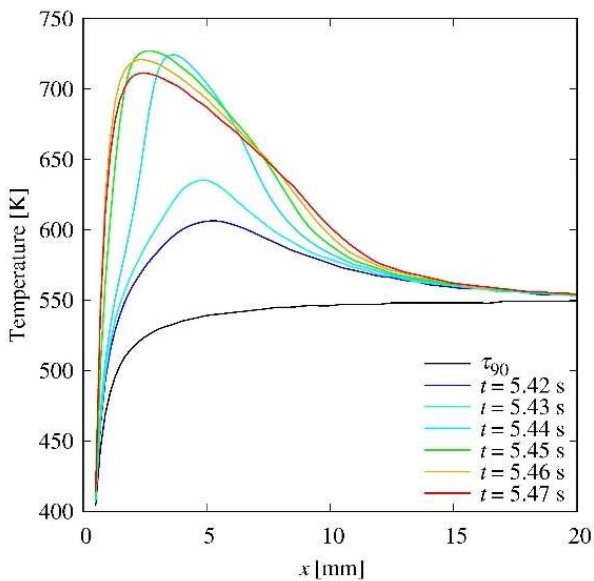


Fig. 9 Time series of temperature along axisymmetric boundary (single droplet).

the droplet surface, temperature decreases while fuel mole fraction increases. According to the **Fig. 6**, the mixture reactivity depends on the temperature and fuel mole fraction has few influence on the reactivity. Therefore, reaction does not progress well due to low temperature in the vicinity of the droplet surface although the fuel concentration is high. After ignition, the ignition propagates inward as the maximum temperature point moves inward as shown in **Fig. 9**. The outside distribution of the fuel mole fraction is sufficient low not to ignite spontaneously while the ambient temperature is high. Thus, it is thought that the ignition propagates inward.

Figure 11 shows the superimposed contours of OH, HCHO, and $OOCC_{10}H_{20}OOH$ mole fractions.

The each color depth of green, blue, and red is assigned to OH, HCHO, and $OOCC_{10}H_{20}OOH$ mole fractions respectively. The contours are ordered in time from (a) to (f). The image (c)

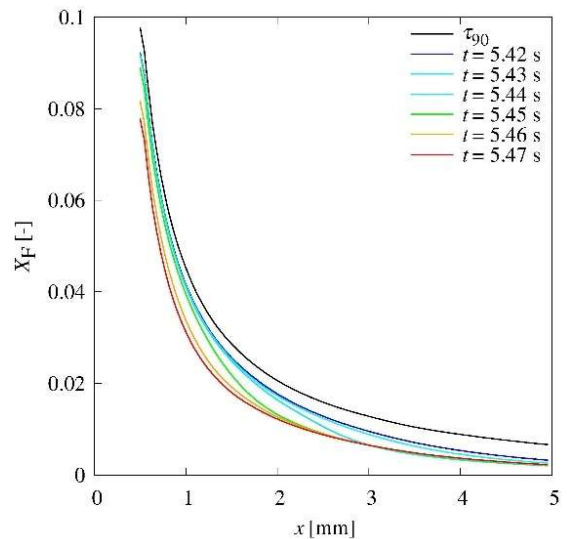


Fig. 10 Time series of the mole fraction of $C_{10}H_{22}$ along axisymmetric boundary (single droplet).

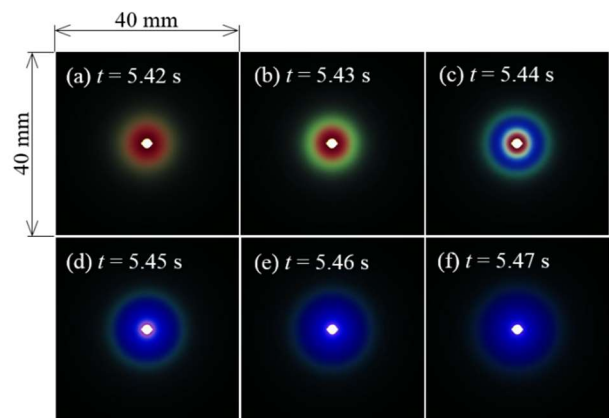


Fig. 11 Superimposed contours of OH (green), HCHO (blue), and $OOCC_{10}H_{20}OOH$ mole fractions (single droplet).

corresponds with the image at the ignition delay time (5.44 s). The interval of each image is 10 ms. The image (a) shows that the $\text{OOC}_{10}\text{H}_{20}\text{OOH}$ is accumulated around the droplet by OH of chain carrier in a looped reaction route. When $\text{OOC}_{10}\text{H}_{20}\text{OOH}$ is accumulated above certain level, the production of OH in the vicinity of the circumference of $\text{OOC}_{10}\text{H}_{20}\text{OOH}$ is found as shown in (b) and HCHO production reaction is activated. At 5.44 s of ignition delay, HCHO production starts concentrically via ketohydroperoxide¹³⁾ from the position where OH mole fraction is high. After then, HCHO spread inward along the radial direction following OH existing between HCHO and $\text{OOC}_{10}\text{H}_{20}\text{OOH}$.

Figure 12 shows the temperature distribution of $D = 8$ mm. In the case of the droplet pair, temperature of inter-droplet region does not rise but temperature rises around droplet pair. The high temperature region proceeds to inward of the droplet pair. The superimposed contours of each intermediate species are shown in **Fig. 13**. Around accumulated $\text{OOC}_{10}\text{H}_{20}\text{OOH}$, OH increases and HCHO is generated rapidly at 5.71 s shown in (C). Since the HCHO generation location and spread direction corresponds with high temperature region and its spread direction, the temperature rising accompanies HCHO generation. As seen in **Fig. 11**, the HCHO production between droplets also delays due to lower temperature than outer temperature.

Figure 14 shows the time series of temperature along axisymmetric boundary. The coordination 3.5 mm to 4.5 mm corresponds with the droplet position. The graph is connected between each value at the calculation node next to the droplet surface node across the droplet position. The temperature at τ_{90} and $x = 0$ mm is 30 K lower than the initial ambient temperature due to low temperature fuel and it leads to weak reaction between droplets. The outer temperature increases at $x = 10.4$ mm which is 5.9 mm away from the droplet surface. On the other hand, the temperature between droplets does not increase much. The outer temperature increases with the temperature peak position shifting inward as well as the single droplet case. At 5.71 s of ignition delay time, the temperature takes maximum at 8.47 mm.

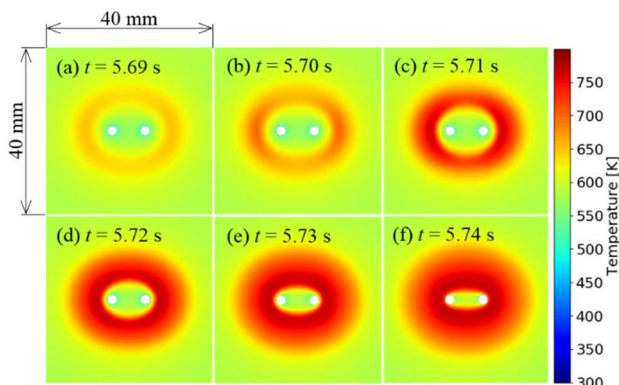


Fig. 12 Contour of temperature ($D = 8$ mm).

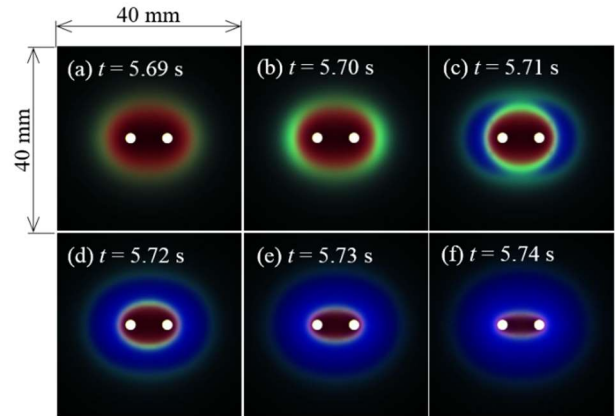


Fig. 13 Superimposed contours of OH (green), HCHO (blue), and $\text{OOC}_{10}\text{H}_{20}\text{OOH}$ (red) mole fractions ($D = 8$ mm).

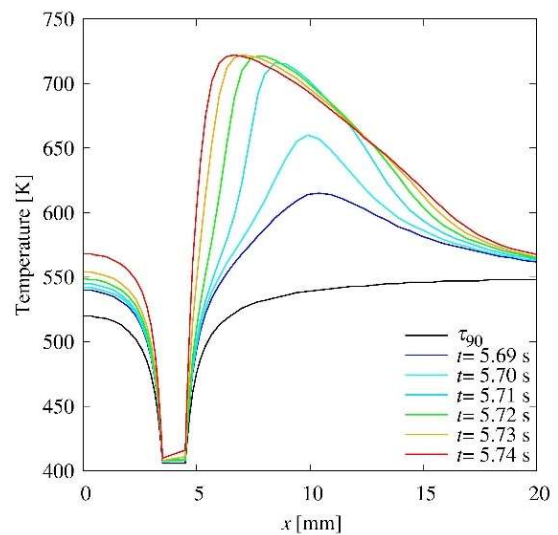


Fig. 14 Time series of temperature along axisymmetric boundary ($D = 8$ mm).

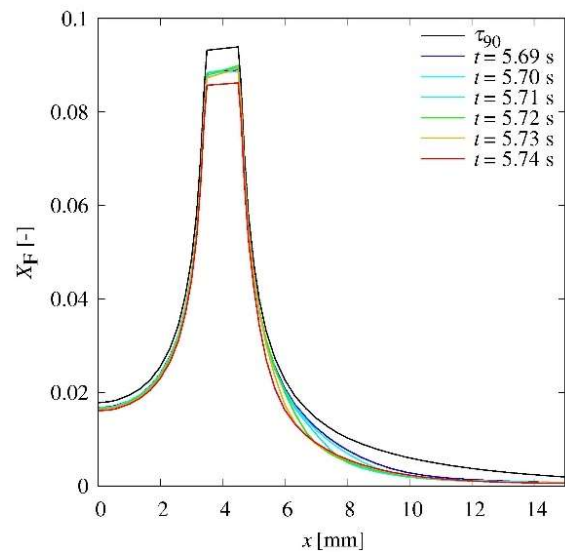


Fig. 15 Time series of the mole fraction of $\text{C}_{10}\text{H}_{22}$ along axisymmetric boundary ($D = 8$ mm).

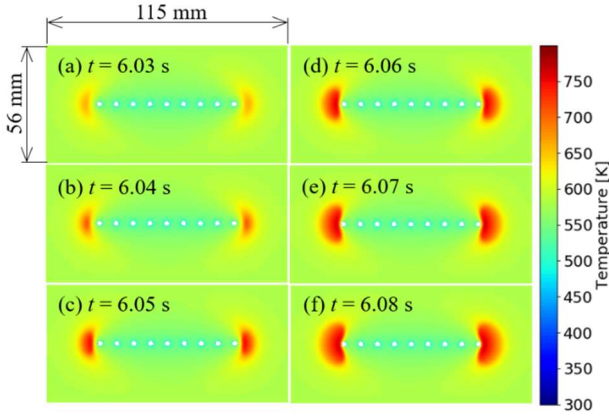


Fig. 16 Contour of temperature (array).

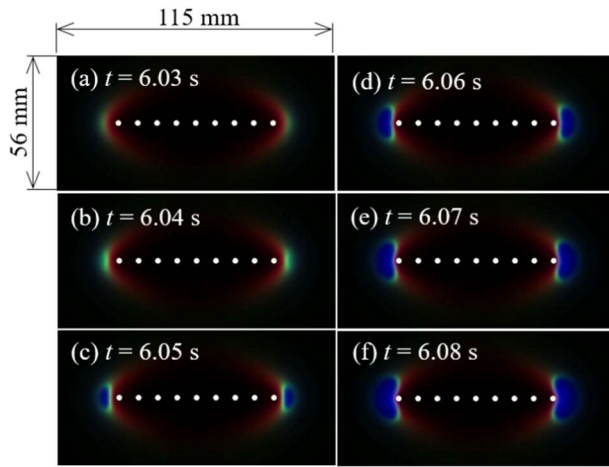


Fig. 17 Superimposed contours of OH (green), HCHO (blue), and OOC₁₀H₂₀OOH (red) mole fractions (array).

Figure 15 shows the time series of the mole fraction of C₁₀H₂₂ along axisymmetric boundary.

The fuel mole fraction in the inter-droplet region is higher than that of the outer region due to fuel flow from each droplet. Between $x = 8 \sim 10$ mm, significant fuel consumption was found and fuel is consumed inward. It can also be found that the temperature rising occurs from the fuel lean side where the temperature is high as well as the single droplet case as shown in **Fig. 10**. The fuel mole fraction and the temperature at the temperature rising position is 0.0054 and 540 K respectively at τ_0 . At the temperature rising position, the slight leaner fuel concentration with the same temperature compared with the single droplet case was found in the case of the droplet pair condition. Although the reason need to be verified in detail, the leaner condition at the outside of the droplets might yield the longer ignition delay compared with the single droplet case.

Figure 16 shows the temperature distribution of the droplet array case.

As shown in (a), temperature starts to increase from the outside of the droplet array. Meanwhile, the temperature between the

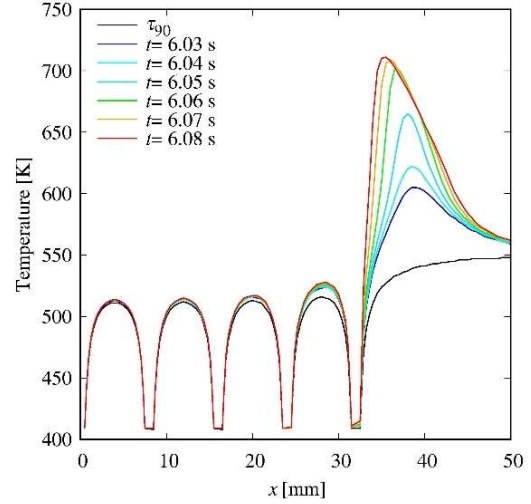


Fig. 18 Time series of temperature along axisymmetric boundary (array).

droplets is still low. At the ignition delay time, high temperature region surrounds the most outer droplet from the outside of the droplet and spreads inward. At this time, the outside high temperature region propagates faster than the inner region. The envelope of the high temperature region as seen in the droplet pair condition of $D = 8$ mm does not be found in the droplet array condition.

Figure 17 shows the superimposed contour of the droplet array. At 0.02 s before the ignition delay time shown in **Fig. 17** (a), OOC₁₀H₂₀OOH is accumulated at the both end of the droplet array. In the next 0.01 s, OH increases at the outside of the OOC₁₀H₂₀OOH. At the ignition delay time shown in (c), HCHO production reaction is activated and HCHO progresses inward following OH. The high temperature region as seen in **Fig. 16** corresponds with the high HCHO region. Thus, the temperature rising caused by the generation of cool flame. Considering low temperature at the inter-droplet region, the spontaneous ignition does not arise within the present calculation time according to **Fig. 6**. Therefore, the cool flame propagates due to heat conduction.

Figure 18 shows the time series of temperature along axisymmetric boundary.

At τ_0 , the inter-droplet temperature is approximate 40 K lower than the initial temperature due to the low temperature fuel flow. At $t = 6.03$ s, temperature starts to rise at $x = 39$ mm. The peak temperature shift inward can be found same as single droplet and droplet pair cases. Fuel mole fraction of the inter-droplet is higher than the outer region as shown in **Fig. 19** as the same tendency to the droplet pair condition. It can be found that the fuel is consumed from the outside of the droplet array. Similar to other two cases, the higher temperature contributes the earlier ignition more considerably than the higher fuel mole fraction. The temperature at τ_0 and the temperature rising position are almost

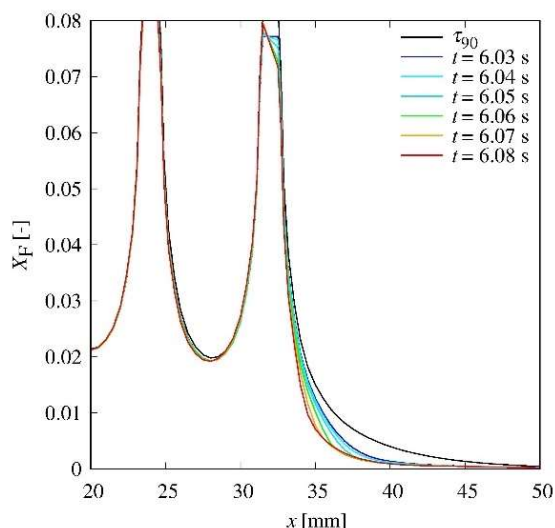


Fig. 19 Time series of the mole fraction of $C_{10}H_{22}$ along axisymmetric boundary (array).

same with the droplet pair condition of inter-droplet distance of 8 mm. On the other hand, the fuel mole fraction was 0.0050 which is slight leaner condition than the $D = 8$ mm condition in spite of the same inter droplet distance. The slight difference of the fuel mole fraction may influence on the ignition delay time.

5. Conclusions

For the prediction of the rocket experiment to clarify the cool flame occurrence, the 2D numerical calculation of the ignition of the single droplet, droplet pair and droplet array is carried out. As a result, the followings are found.

1. The ignition delay time becomes long with decrease in the inter-droplet distance. The slight difference of the fuel concentration at the temperature rising position was found between the single droplet, droplet pair, and droplet array which show different ignition delay times. On the other hand, almost same temperature was found at the temperature rising position. It can be explained that the slight difference of the fuel concentration may influence on the ignition delay time.

2. From the 2D calculation, it is found that the outside of the fuel droplet pair and droplet array take high temperature and low fuel concentration while the inner regions take low temperature

and high fuel concentration. The 0D reaction calculation shows that the influence of the low temperature due to fuel flow on the ignition delay time is larger than that of high fuel concentration near droplet. Therefore, it is thought that the ignition occurs at the outside of the droplets where the fuel concentration is low and the temperature is high.

Acknowledgement

The figures of the DCU were supplied by IHI Inspection & Instrumentation Co., Ltd. This study is supported by ISAS-JAXA as *The Front-Loading Project*.

References

- 1) Y. Iwabuchi, K. Kawai, T. Shoji and Y. Takeda: SAE Technical Paper, **26** (1996) 1637.
- 2) M. Tanabe, M. Kono, J. Sato, J. Koenig, C. Eigenbrod, F. Dinkelacker and H. J. Rath: J. Combust. Sci. Technol., **108** (1995) 103.
- 3) M. Tanabe, M. Kono, J. Sato, J. Koenig, C. Eigenbrod and H.J. Rath: Proceedings of the Combustion Institute, (1994) 455.
- 4) S. Kumagai, and H. Isoda: Proceedings of the Combustion Institute, (1957) 726.
- 5) O. Moriue, Y. Nishiyama, Y. Yamaguchi, H. Hashimoto and E. Murase: Proceedings of the Combustion Institute, **34** (2013) 1585.
- 6) C. Eigenbrod, K. Klinkov, M. Peters, G. Marks, W. Paa, V. Wagner and W. Triebel: Int. J. Microgravity Sci. Appl., **33** (2016) 330306.
- 7) M. Kikuchi, S. Yamamoto, S. Yoda, M. Mikami, H. Nomura, O. Moriue, A. Umemura, Y. Hisashi, N. Sugano, K. Moesl, T. Sattelmayer, C. Eigenbrod and O. Minster: Proc. 20th ESA Symposium on European Rocket and Balloon Programmes and Related Reserch, (2011) 473.
- 8) M. Mikami, M. Kikuchi, Y. Kan, T. Seo, H. Nomura, Y. Sukanuma, O. Moriue and D L Dietrich: Int. J. Microgravity Sci. Appl., **33** (2016) 330208.
- 9) M. Mikami, H. Nomura, Y. Sukanuma, M. Kikuchi, T. Suzuki and M. Nokura: Int. J. Microgravity Sci. Appl., **35** (2018) 350202.
- 10) Y. Yoshida, N. Sano, T. Seo, M. Mikami, O. Moriue, Y. Kan and M. Kikuchi: Int. J. Microgravity Sci. Appl., **35** (2018) 350203.
- 11) T I. Farouk and F.L. Dryer: Combustion and Flame, **161** (2014) 565.
- 12) T. I. Farouk, M. C. Hicks and F. L. Dryer: Proceedings of the Combustion Institute, **35** (2015) 1701.
- 13) M. Saito, Y. Sukanuma, M. Mikami, M. Kikuchi, Y. Inatomi, O. Moriue, H. Nomura and M. Tanabe: JASMAC-29, (2017) 27A05.
- 14) H. Nomura, T. Murakoshi, Y. Sukanuma, Y. Ujiiie, N. Hashimoto and H. Nishida: Proceedings of the Combustion Institute, **36** (2017) 2425.
- 15) L. Qiu, X. Cheng, X. Wang, Z. Li, Y. Li, Z. Wang and H. Wu: Energy & Fuels, **30** (2016) 10875.
- 16) C. Chauveau, M. Birouk and I. Gökalp: Int. J. Multiphase Flow, **37** (2011) 252.